The von Hippel-Lindau tumor suppressor protein controls ciliogenesis by orienting microtubule growth

Bernhard Schermer,[1] Cristina Ghenoiu,[1] Malte Bartram,[1] Roman Ulrich Müller,[1] Fruzsina Kotsis,[1] Martin Höhne,[1] Wolfgang Kühn,[1] Manuela Rapka,[1] Roland Nitschke,[3] Hanswalter Zentgraf,[4] Manfred Fliegauf,[2] Heymut Omran,[2] Gerd Walz,[1] and Thomas Benzing[1]

[1]Renal Division and [2]Children's Hospital, University Hospital Freiburg, 79106 Freiburg, Germany
[3]Life Imaging Center, Institute of Biology, University of Freiburg, 79104 Freiburg, Germany
[4]Deutsches Krebsforschungszentrum, 69120 Heidelberg, Germany

Cilia are specialized organelles that play an important role in several biological processes, including mechanosensation, photoperception, and osmosignaling. Mutations in proteins localized to cilia have been implicated in a growing number of human diseases. In this study, we demonstrate that the von Hippel-Lindau (VHL) protein (pVHL) is a ciliary protein that controls ciliogenesis in kidney cells. Knockdown of pVHL impeded the formation of cilia in mouse inner medullary collecting duct 3 kidney cells, whereas the expression of pVHL in VHL-negative renal cancer cells rescued the ciliogenesis defect. Using green fluorescent protein–tagged end-binding protein 1 to label microtubule plus ends, we found that pVHL does not affect the microtubule growth rate but is needed to orient the growth of microtubules toward the cell periphery, a prerequisite for the formation of cilia. Furthermore, pVHL interacts with the Par3–Par6–atypical PKC complex, suggesting a mechanism for linking polarity pathways to microtubule capture and ciliogenesis.

Introduction

The tumor syndrome von Hippel-Lindau (VHL) disease is caused by heterozygous germline inactivation of the *VHL* tumor suppressor gene, which resides on chromosome 3p25 (Kaelin, 2003). The cardinal feature of this hereditary cancer syndrome is the development of multiple vascular tumors called hemangioblastomas in the central nervous system and retina combined with clear cell carcinoma of the kidney and pheochromocytoma. VHL disease is an autosomal-dominant disorder, and tumor development in VHL disease is linked to somatic inactivation of the remaining wild-type *VHL* allele, leading to loss of the wild-type *VHL* gene product, VHL protein (pVHL). In the kidney, this event not only precipitates the development of clear cell carcinoma but is also associated with the growth of premalignant renal cysts (Lubensky et al., 1996; Mandriota et al., 2002). Restoration of pVHL expression is sufficient to suppress kidney tumor formation by pVHL-defective renal carcinoma cells in vivo, suggesting that tumorigenesis is a direct effect of the loss of both *VHL* alleles (Iliopoulos et al., 1995; Schoenfeld et al., 1998). Despite recent advances in our understanding of pVHL function in tumor formation (Kaelin, 2003; Ratcliffe, 2003), the pathogenesis of cystic kidney disease in VHL patients remains unknown.

Recently, the molecular pathogenesis of other cystic kidney diseases has been linked to the monocilia of kidney cells (Benzing and Walz, 2006). Cilia are highly conserved organelles that project from the surfaces of many cells (Igarashi and Somlo, 2002). The essential structure of renal monocilia consists of nine peripheral microtubule doublets forming the axoneme and surrounded by a membrane lipid bilayer that is continuous with the plasma membrane. The ciliary axoneme emerges from the basal body, a microtubule-based structure that also functions as the spindle-organizing center in mitosis. Cilia are sensory organelles (Snell et al., 2004; Pan et al., 2005), and it has been demonstrated that renal monocilia are involved in mechanosensation (Nauli et al., 2003; Praetorius and Spring,

B. Schermer, C. Ghenoiu, and M. Bartram contributed equally to this paper.

Correspondence to Thomas Benzing: thomas.benzing@uniklinik-freiburg.de

Abbreviations used in this paper: aPKC, atypical PKC; EB1, end-binding protein 1; HEK, human embryonic kidney; IFT, intraflagellar transport; mIMCD, mouse inner medullary collecting duct; pVHL, VHL protein; RCC, renal cell carcinoma; shRNA, short hairpin RNA; UTR, untranslated region; VHL, von Hippel-Lindau.

The online version of this article contains supplemental material.

The Journal of Cell Biology, Vol. 175, No. 4, November 20, 2006 547–554
http://www.jcb.org/cgi/doi/10.1083/jcb.200605092

2003a,b). The assembly and maintenance of cilia are mediated by intraflagellar transport (IFT), a bidirectional microtubule-based transport system.

In this study, we demonstrate that pVHL localizes to the monocilia of kidney cells and controls ciliogenesis. Furthermore, we show that pVHL is essential for the oriented growth of microtubules toward the cell periphery, a prerequisite for the formation of cilia. Moreover, pVHL interacts with the Par3–Par6–atypical PKC (aPKC) polarity complex, suggesting that pVHL may connect Par3–Par6–aPKC polarity proteins to microtubule capture and ciliogenesis. Our results uncover a novel role for pVHL that links the pathogenesis of premalignant renal cysts in VHL disease with the role of kidney cell monocilia in cystogenesis.

Results and discussion

We examined the localization of pVHL in polarized kidney cells using different anti-pVHL antisera. Renal tubular epithelial cells (MDCK clone II) were grown on cell culture inserts for a minimum of 5 d after confluence to allow complete epithelial polarization. We observed specific staining in the cytoplasm of the cells and some nuclear staining, as described previously (Hergovich et al., 2003; and unpublished data). In addition, strong pVHL staining in monocilia was detected by several pVHL antibodies (Fig. 1). Cilia were identified with an antiacetylated tubulin antibody, which is a marker of the ciliary axoneme (Fig. 1, a and b). pVHL staining was completely blocked by adding an excess of recombinant pVHL peptide, confirming the staining specificity (Fig. 1 b). The same pVHL localization was observed using anti-pVHL antibody and anti–rabbit AlexaFluor-conjugated antisera but omitting the antiacetylated tubulin antisera, excluding cross-reactivity or bleed-through of the fluorescent label. No immunofluorescence was detected when secondary antibodies were used alone (unpublished data).

Double and triple labeling of native human respiratory epithelial cells revealed that pVHL is also present in motile cilia of respiratory epithelial cells (Fig. S1, available at http://www.jcb.org/cgi/content/full/jcb.200605092/DC1). pVHL was detected in the ciliary axoneme (costained with antibodies against acetylated tubulin) and basal bodies (costained with antibodies against γ-tubulin). Immunoelectron microscopy of respiratory epithelial cells revealed that pVHL staining was confined to protein complexes associated with the ciliary microtubules (Fig. S1 c). These data suggested that pVHL may be important for the formation or maintenance of cilia and prompted us to examine the effect of *VHL* deletion on ciliogenesis.

To address a possible role for pVHL in the formation or maintenance of cilia, we examined ciliogenesis in pVHL-deficient and in wild-type kidney cells. The A498 renal cell carcinoma (RCC) cell line contains a single VHL allele with a frameshift mutation at codon 142, leading to the expression of a defective C-terminally truncated pVHL (Gnarra et al., 1994). Lentiviral vectors containing V5-tagged human $pVHL_{30}$ cDNA or an empty cassette (control) were used to transduce pVHL-deficient A498 RCC cells. The reexpression of pVHL was confirmed by immunoblotting with anti-V5 antibody (Fig. 2 a).

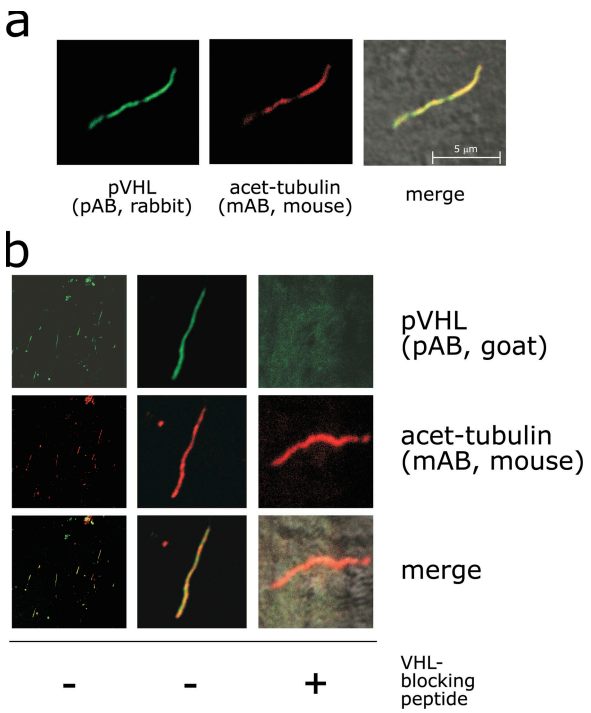

Figure 1. **pVHL is localized to renal monocilia.** (a) Colocalization of pVHL and acetylated tubulin in primary cilia of MDCK cells. MDCK cells were grown on coverslips at 100% confluence and cultured for 5 d before the experiment to allow full polarization and cilia formation. Localization of pVHL was determined by immunofluorescence using a pVHL-specific antibody (green, rabbit polyclonal; sc-5575) with confocal images captured at the level of the apical membrane. Cells were costained with mouse antiacetylated tubulin antibody (middle), a marker protein for cilia. All images were captured using sequential Cy3 and AlexaFluor488 scans on a laser confocal microscope to eliminate bleed-through signals from the green and red fluorescence. (b) Specific localization of pVHL in primary cilia was confirmed by the use of an additional anti-VHL antibody (goat polyclonal; sc-1535) and blocking with recombinant pVHL. Lower magnification (left) and higher magnification views (middle) of ciliated cells are shown. Incubation of the specific pVHL antibody with a blocking recombinant protein (10-fold excess) resulted in the loss of pVHL staining in cilia, demonstrating specificity of the antibody stain (right).

VHL-defective and -positive cells were grown 10 d after confluence to allow epithelial polarization and cilia formation. Under the chosen conditions, VHL-negative cells did not assemble cilia. Even after >14 d after confluence, control cells transduced with empty lentivirus did not form cilia (visualized with antiacetylated tubulin antibodies; Fig. 2, b and c). In contrast, the lentivirally mediated reexpression of pVHL resulted in the formation of intact monocilia at the apical surface of the cells, suggesting that pVHL expression is essential for cilia formation. Ciliogenesis was quantified by blinded counting of cilia in two independent experiments (Fig. 2 b). Similar to wild-type cells, pVHL-reexpressing cells showed a ciliary localization of pVHL, as demonstrated by the costaining of pVHL with the cilia marker protein acetylated tubulin (Fig. 2 c). Reexpressed pVHL could also be stained with anti-V5 antibody, confirming specific staining in monocilia (Fig. S2 a, available at http://www.jcb.org/cgi/content/full/jcb.200605092/DC1).

Next, we engineered a cell line that expressed VHL under the control of a tetracyclin-dependent promoter. VHL-negative

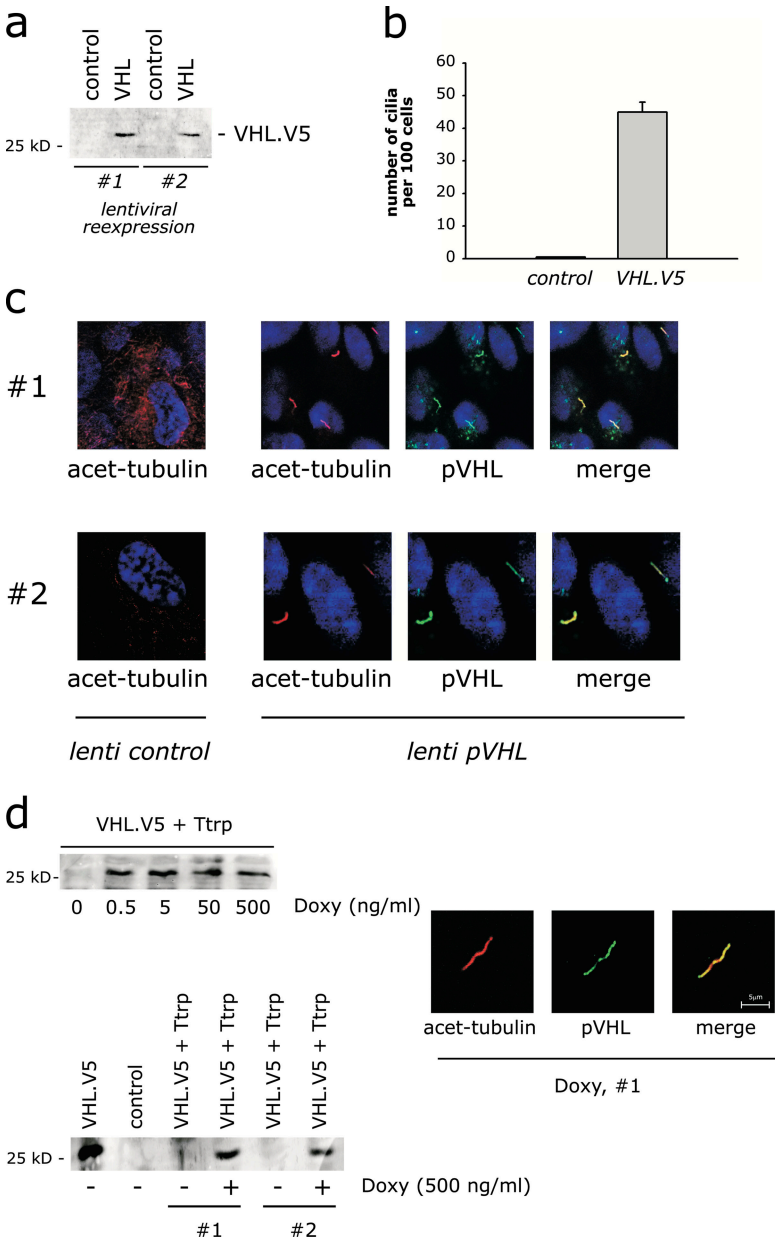

Figure 2. **Lentivirally mediated reexpression of pVHL rescues the cilia-defective phenotype of VHL-negative renal epithelial cells.** (a) Lentiviral vectors containing human $pVHL_{30}$ cDNA or an empty cassette were generated and used to infect VHL-defective A498 RCC cells. Reexpression of pVHL was confirmed by immunoblotting with VHL-specific antibody. #1 and #2 denote two different pools of transduced cells. (b) Ciliogenesis was quantified by blinded counting of cilia in two independent experiments (three slides each). Error bars represent SD. (c) VHL-defective (left; lentiviral control) and -positive cells (right; lentiviral pVHL) were grown 10 d after confluence to allow epithelial polarization and cilia formation. Red, acetylated tubulin; green, reexpressed V5-tagged pVHL; merge in the far right panels. (d) Doxycycline-induced reexpression of pVHL in tet-inducible A498 cells. Ttrp denotes the lentivirally mediated expression of Tet repressor. Top panel shows a dose-response curve (24 h of incubation). Doxycycline-mediated pVHL expression is shown (bottom) and results in the formation of cilia in pVHL-expressing cells (right). Reexpressed pVHL was stained with an anti-V5 antibody.

A498 cells were lentivirally transduced to express a tet repressor together with a tet-dependent VHL construct. Incubation of the cells in the presence of doxycycline resulted in pVHL expression already at very low doxycycline concentrations (Fig. 2 d). Several independent clones of cells were generated, plated at high density, and grown on cell culture inserts in the absence and presence of 500 ng/ml doxycycline for 5 d. As demonstrated in the previous paragraph, VHL-negative cells did not show cilia formation under the conditions chosen (unpublished data). In contrast, doxycyclin-treated cells displayed the formation of monocilia (~10% of cells). These monocilia again stained positive for pVHL (as demonstrated by stainings with an anti-V5 antibody; Fig. 2 d).

To further study a role for pVHL in the formation of cilia, we next searched for short hairpin RNAs (shRNAs) to interfere with VHL expression in renal cells. To test the efficacy of candidate shRNAs, the cDNA of mouse *VHL* (coding sequence plus 3′ untranslated region [UTR]) was cloned into a bicistronic luciferase vector to fuse this cDNA with the coding sequence of *Renilla reniformis* luciferase. In this system, the activity of the *R. reniformis* luciferase is a quantitative parameter of RNA degradation mediated by cotransfected shRNAs. Coexpressed firefly (*Photinus pyralis*) luciferase served as a control to normalize for transfection efficiency, expression level, and cell number. Several shRNAs were synthesized based on publicly available prediction programs (Table I; Yuan et al., 2004). These reagents were then tested by sequentially measuring the activities of firefly and *R. reniformis* luciferases in a 96-well format (Fig. S3 a, available at http://www.jcb.org/cgi/content/full/jcb.200605092/DC1). shRNA#3 resulted in an almost 70% knockdown of the reporter construct (Fig. S3 a) and efficient knockdown of the mouse pVHL (Fig. S3 b). We used shRNA#3 cloned into a lentivirus

Table I. **Sequence information for hairpin constructs**

Hairpin	DNA sequence[a]	Target
mVHL #1	G**AGAAGATGACCTGAGAGGGCT**GTTTTGGCCACTGACTGACAGCCCTCTGGTCATCTTCT	cds
mVHL #2	G**TTAACCAGAAGTCCATCATGG**GTTTTGGCCACTGACTGACCCATGATGCTTCTGGTTAA	cds
mVHL #3	G**AACTCAGGAACACTTAATCTC**GTTTTGGCCACTGACTGACGAGATTAAGTTCCTGAGTT	3′ UTR
mVHL #4	G**AACACTACAAAGCCCAGGGAT**GTTTTGGCCACTGACTGACATCCCTGGTTTGTAGTGTT	3′ UTR
mVHL #5	G**TTAAACACTACAAAGCCCAGG**GTTTTGGCCACTGACTGACCCTGGGCTGTAGTGTTTAA	3′ UTR
hsaVHL #1	G**TAAGGAAGGAACCAGTCCTGT**GTTTTGGCCACTGACTGACACAGGACTTTCCTTCCTTA	3′ UTR
Scrambled	G**AAATGTACTGCGCGTGGAGAC**GTTTTGGCCACTGACTGACGTCTCCACGCAGTACATTT	None

cds, coding sequence.
[a]Without overhangs; antisense target sequences (mature micro-RNA sequence) are indicated in bold.

vector to selectively knockdown VHL expression in mouse inner medullary collecting duct 3 (mIMCD3) kidney cells. shRNA expression was monitored by simultaneous coexpression of GFP from the same construct (Fig. S3 c). This strategy allows the identification of cells that effectively express shRNA. Interestingly, this level of knockdown was not associated with a marked change in the growth rate of the cells. Cell growth and formation of a closed monolayer was indistinguishable in cells with and without VHL knockdown, suggesting that low levels of pVHL are sufficient to prevent tumorlike cell growth. The lentivirally mediated expression of shRNA#3 against VHL but not of a control scrambled shRNA inhibited cilia formation, supporting the concept that pVHL controls ciliogenesis. Identical results were obtained with shRNA#2 (unpublished data). Importantly, although cilia formation was greatly attenuated in VHL knockdown cells, ciliogenesis was not entirely abrogated in this assay (some cilia could form at later stages).

Next, we examined the mechanism by which pVHL may affect ciliogenesis. The essential structure of cilia consists of nine peripheral microtubule doublets forming the axoneme and surrounded by a membrane lipid bilayer that is continuous with the plasma membrane (Rosenbaum and Witman, 2002). In microtubule sedimentation experiments, we found that pVHL associates with microtubules (Fig. 3 a), and immunoprecipitation experiments revealed that pVHL interacts with β-tubulin (Fig. 3 b). Thus, it appears that pVHL is associated with microtubules. But how could this protein play a role in ciliogenesis? One possible explanation is that pVHL may have a direct effect on microtubule stability, as has been described previously by Hergovich et al. (2003). We tested this possibility by treating VHL-positive and -negative cells with 20 μM of the microtubule-depolarizing drug nocodazole for 20 min, staining the cells with antiacetylated tubulin antibody, and checking for the integrity of microtubules by fluorescence microscopy. We were particularly interested in an effect on the peripheral microtubule network. However, we could not find an obvious defect in microtubule stability in VHL-negative cells or rescue from microtubule instability in pVHL-reexpressing cells (unpublished data).

Alternatively, pVHL might influence microtubule growth rates or their directionality and organization. To test this possibility, we examined microtubule growth and directionality using end-binding protein 1 (EB1) tagged with GFP in VHL-positive and -negative cells by high speed time-lapse videos. EB1 and

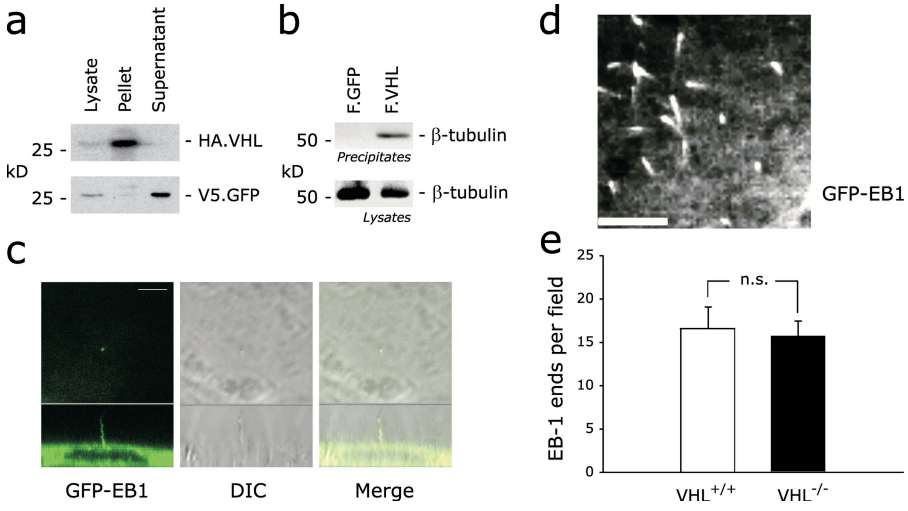

Figure 3. **pVHL associates with microtubules but does not affect microtubule growth or stability.** (a) pVHL binds microtubules. Microtubules were polymerized in vitro, and supernatants and microtubule pellets were then subjected to SDS-PAGE and immunoblotted for the indicated proteins. (b) β-Tubulin coprecipitates with pVHL. FLAG-tagged pVHL (F.VHL) or a control protein (F.GFP) were expressed in HEK 293T cells and precipitated with anti-FLAG antibody. Western blot analysis was performed with a β-tubulin–specific antibody (top). Expression levels of β-tubulin in the lysates are shown (bottom). (c) End-binding protein 1 (EB1) tagged with GFP tracks microtubule growth in the monocilia of kidney cells, suggesting that this protein is a suitable reagent to study the microtubule formation required for ciliogenesis. GFP-EB1 was expressed in MDCK cells, and fluorescence (1,024 × 1,024 pixels) as well as differential interference contrast (DIC) images were recorded with a confocal scanning microscope. The confocal pinhole was set to achieve an optical slice thickness of 0.9 μm (top). The bottom panel shows a z stack of the same area. (d) GFP-EB1 accumulates at the plus ends of microtubules. GFP-EB1 movements were visualized with high speed confocal microscopy. (e) VHL does not affect the number of growing microtubules at the cell cortex. To estimate the number of growing microtubules at the cell cortex, GFP-EB1–positive microtubules were counted at the cell periphery in defined areas of interest and were compared in VHL-positive and -negative cells ($n = 8$). Tracking paths were measured in two square fields (256 μm^2) per cell positioned in the cytosol adjacent to the plasma membrane. Error bars represent SD. Bars, 5 μm.

its *Caenorhabditis elegans* homologue EBP-2 have been shown to decorate the plus ends of growing microtubules (Salaycik et al., 2005; Srayko et al., 2005) and, thus, can be used to dynamically monitor microtubule formation (Mimori-Kiyosue et al., 2000). GFP-EB1 decorates the microtubules of cilia (Fig. 3 c), suggesting that this protein is a suitable reagent to study the microtubule formation required for ciliogenesis. Targeting to cilia is specific to GFP-EB1 and could not be demonstrated with GFP alone (Fig. S2 b). However, because VHL-negative cells do not form cilia, studies addressing the microtubule formation required for ciliogenesis have to be performed in the cytoplasm.

We reasoned that monitoring microtubule formation at the cell cortex may allow us to address the mechanism that leads to the ciliogenesis defect in VHL-negative cells. In fact, this is what we found. Using life confocal microscopy, we observed multiple small dots of fluorescence moving at the cell periphery in both VHL-positive and -negative cells (Fig. 3 d and Videos 1 and 2; available at http://www.jcb.org/cgi/content/full/jcb.200605092/DC1). The number of forming microtubules at the cell cortex did not differ in VHL-negative cells (Fig. 3 e). To study the direction and growth rate of microtubules, fluorescent GFP-EB1 dot movements were tracked over 10 s in high speed time-lapse videos using MetaMorph software; microtubule growth rates and direction were determined from these data. Examples of microtubule growth tracks are shown in Fig. 4 a. To exclude the possibility that differentiation plays a major role in the effect of pVHL on microtubule growth, the experiments were performed in nonpolarized, nonconfluent cells (EB1-GFP–expressing A498 cells rescued with V5.lacZ or V5.VHL). The analyzed region of interest was chosen between the centrosome and the cell membrane. In undifferentiated cells, the centrosome is located near the nucleus, whereas in fully differentiated cells, the centrosome localizes to the apical membrane, where the cilium originates. Only undifferentiated cells with centrosomes close to the nucleus were taken for the analyses, excluding the possibility that polarization, reorientation of centrioles, changes in microtubular polarity, or marked differences in cell cycle progression are responsible for any of the effects observed.

As stated in the previous paragraph, we found no obvious difference in microtubule growth between VHL-positive and -negative cells. However, we noticed that in wild-type cells, the direction of growth of newly formed microtubules at the cell periphery is coordinated toward the outer plasma membrane, whereas in VHL-deficient cells, growth directions appear to be less coordinated (Fig. 4, a and b). To perform a statistical analysis of the directionality of microtubule growth in regions of interest in different cells, the microtubule growth directions were expressed as the deviation from a calculated sum vector of all growth directions in one particular experiment. The summary of five independent experiments revealed a statistically significant difference in deviation from the sum vectors in VHL-negative cells (Fig. 4 c), demonstrating that VHL deficiency affects the coordinated growth of microtubules. These data suggest that the deficiency in ciliogenesis in VHL-negative cells may be a result of the uncoordinated growth of microtubules.

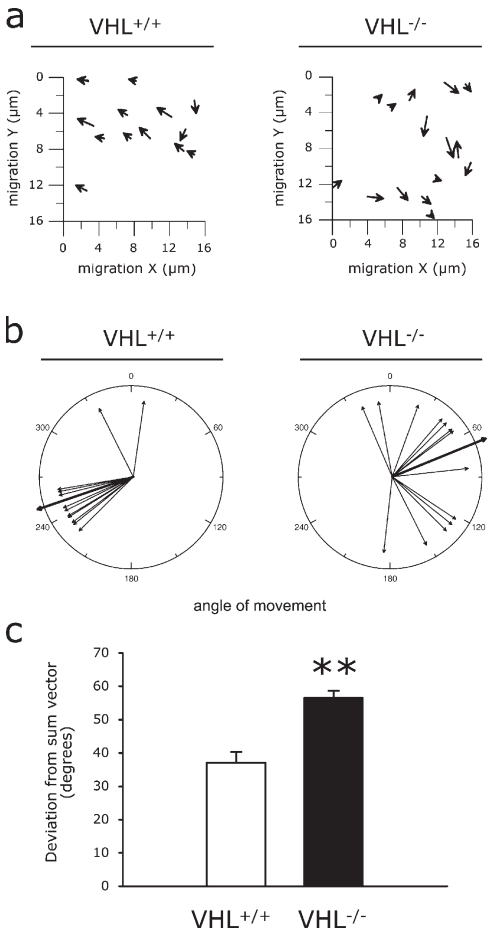

Figure 4. **VHL deficiency affects the directed growth of microtubules.** (a) Representative trackings of EB1 tagged with GFP (GFP-EB1) in the cytoplasm of VHL-positive and -negative cells. Each trace represents the history of GFP-EB1 movement (microtubule growth) over sequential time frames with an acquisition rate of two images per second. (b) Microtubule growth events were expressed as the deviation from the mean angle (depicted as the sum vector in bold) in VHL-positive and -negative cells. A representative experiment of five independent analyses is shown. (c) Tracking paths were measured in one to two square fields (256 μm^2) positioned in the cytosol in a total of 10 independent experiments (VHL negative and positive). As a measure for directed or nondirected movement, the deviation of the individual growth angles from the mean angle was calculated in each square. Statistical analysis was performed for VHL-positive and -negative cells using the two-tailed *t* test (**, $P < 0.01$). Error bars represent the SEM.

Members of the family of Ras-related Rho GTPases have emerged as key regulators controlling microtubule–cortex interactions and the coordinated growth of cortical microtubules (Gundersen et al., 2004; Jaffe and Hall, 2005). Three critical effectors of the GTPase-mediated microtubule control have been identified, including Par6 (Etienne-Manneville and Hall, 2003), IQGAP1 (Fukata et al., 2002; Watanabe et al., 2004), and the mammalian homologue of Diapharous (mDia1; Palazzo et al., 2001). Interestingly, coimmunoprecipitation experiments revealed a specific interaction of pVHL with Par6 (Fig. 5 a). pVHL precipitated the Par3–Par6–PKCζ protein complex in human embryonic kidney (HEK) 293T cells (Fig. 5 b). Immunoprecipitation of endogenous pVHL from the mouse kidney demonstrated that pVHL is in a complex with Par3, Par6, and

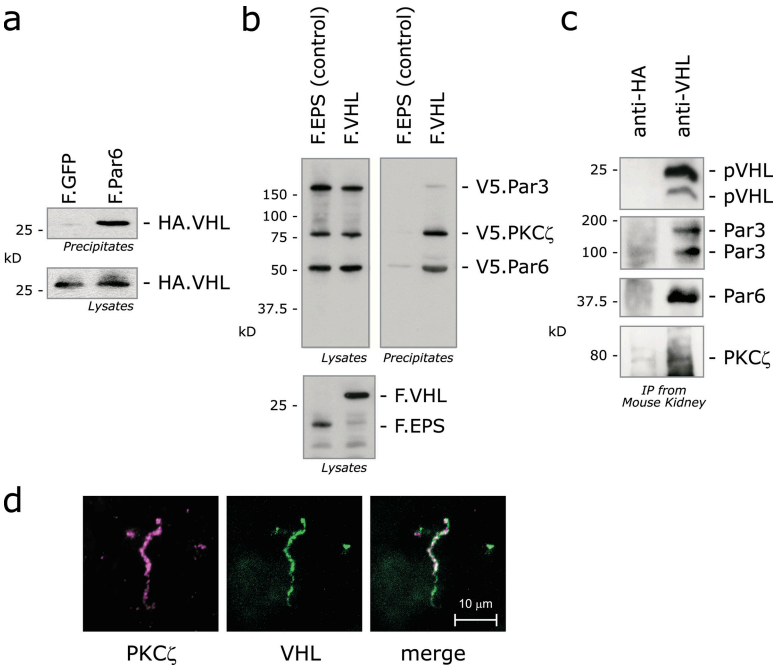

Figure 5. **pVHL interacts with the Par3–Par6–aPKC polarity complex.** (a) VHL coprecipitates with Par6. FLAG-tagged Par6 (F.Par6) or a control protein (F.GFP) were coexpressed with HA-tagged VHL (HA.VHL) in HEK 293T cells and precipitated with anti-FLAG antibody. Western blot analysis was performed with anti-HA antibody (top). Expression levels of HA.VHL in the lysates are shown (bottom). (b) pVHL precipitates the Par3–Par6–aPKC protein complex. V5-tagged Par6 (V5.Par6), Par3 (150-kD isoform; V5.Par3), and aPKC (V5.PKCζ) were coexpressed with FLAG-tagged VHL or a control protein (F.EPS) in HEK 293T cells. pVHL and the control protein were precipitated with anti-FLAG antibody, and coprecipitating Par3, Par6, and PKCζ were visualized with anti-V5 antibody on Western blots (right). Expression levels of all proteins in the lysates are shown (left and bottom). (c) Native pVHL from mouse kidney lysates coprecipitates the Par3–Par6–aPKC protein complex. Freshly isolated mouse kidneys were perfused with ice-cold PBS, lysed, and subjected to immunoprecipitation with control or anti-pVHL antibodies. Precipitated pVHL and coprecipitating proteins were detected with specific antibodies. (d) Colocalization of pVHL and aPKC (PKCζ) in primary cilia of MDCK cells. MDCK cells were grown on Transwell filters (0.4-μm pore size; polyesther; Corning) at 100% confluence and cultured for 5 d before the experiment to allow full polarization and cilia formation.

aPKC in vivo (Fig. 5 c). Moreover, aPKC (PKCζ) colocalized with pVHL in the monocilia of MDCK cells (Fig. 5 d). Collectively, these data suggest that Par3– Par6–aPKC and pVHL may operate in the same pathway to regulate the cortical growth of microtubules and the formation of cilia.

Recently, the Par3–Par6–aPKC polarity proteins have been shown to localize to cilia and interact with the anterograde IFT motor kinesin-2, linking polarity proteins with IFT, microtubules, and the formation of cilia (Fan et al., 2004). However, the exact mechanisms of how ciliogenesis, IFT, and polarity proteins may be intertwined remained elusive. We now show that pVHL also localizes to cilia, interacts with Par3–Par6–aPKC, and controls ciliogenesis. Although we failed to detect kinesin-2 components in the complex (unpublished data), our data demonstrating a critical role for pVHL in controlling the growth direction of microtubules suggest a common function of pVHL, polarity proteins, and IFT in controlling microtubular orientation and dynamics. This adds another aspect to an important role for pVHL in regulating the microtubule cytoskeleton in cells. Previous studies showed that pVHL stabilizes microtubules (Hergovich et al., 2003) and influences microtubule dynamics at the periphery of living cells (Lolkema et al., 2004). We now demonstrate that pVHL is critically involved in regulating the orientation of microtubular growth at the cell periphery. Because pVHL also interacts with Par6, which is a key regulator of microtubule–cortex interactions and the coordinated growth of cortical microtubules (Etienne-Manneville and Hall, 2003), it is conceivable that pVHL and Par6 are in a common pathway to regulate microtubule orientation. Well-regulated microtubule orientation is a prerequisite for ciliogenesis, so the function of pVHL in controlling cilia formation may be the result of a common function of pVHL, polarity proteins, and IFT in controlling microtubule dynamics in the cell. Future studies will have to address the question of how pVHL, polarity proteins, and IFT regulate microtubule dynamics independently of ciliogenesis.

These data assign a novel role for the tumor suppressor pVHL and have important implications for the understanding of VHL disease. A critical role of pVHL in regulating ciliogenesis has also been documented by others (Esteban et al., 2006; Lutz and Burk, 2006) and could explain why VHL patients can develop polycystic kidney disease. Although much has been learned about the function of pVHL in tumorigenesis at the molecular level, the pathogenesis of premalignant kidney cysts in VHL patients has remained elusive (Kaelin, 2004). Thus, our finding that pVHL plays a critical role in ciliogenesis sheds new light on the pathogenesis of premalignant kidney cysts in VHL patients.

Materials and methods

Plasmids and antibodies

HA- and FLAG-tagged human VHL constructs were provided by S.A. Karumanchi (Harvard Medical School, Boston, MA). Human VHL was cloned into pLenti6.V5/Dest and pLenti4/TO/V5/Dest (Invitrogen) using GATEWAY cloning technology. Mouse VHL (coding sequence and 3′ UTR) was PCR cloned from the full-length clone IRAV-6402536 (Open Biosystems) into a modified GATEWAY pENTR1A vector, and recombination was performed into pcDNA3.1.nV5.Dest to obtain V5.mVHL. GATEWAY vectors and lentiviral constructs were obtained from Invitrogen or were provided by T. Tuschl and M. Landthaler (Rockefeller University, New York, NY), D. Trono (University of Geneva, Geneva, Switzerland), and L. Naldini (University of Torino, Torino, Italy). EB1-GFP was provided by Y. Mimori-Kiyosue (KAN Research Institute, Kyoto, Japan; Mimori-Kiyosue et al., 2000). Site-directed mutagenesis was performed using the QuikChange Site-Directed Mutagenesis Kit (Stratagene). All plasmids were verified by automated DNA sequencing. Antibodies were obtained from Sigma-Aldrich (anti-FLAG, antiacetylated tubulin, and anti-PKCζ), Santa Cruz Biotechnology, Inc. (anti-myc, anti-HA, anti-VHL pAb, and anti-Par6), Oncogene Research Products (anti-VHL mAb), Serotec (anti-V5 mAb), Covance (anti-HA pAb), and Roche Biochemicals (anti-HA mAb).

Cell culture and transfections

HEK 293T cells were cultured in DME supplemented with 10% FBS. For transfection experiments, cells were grown until 60–80% confluence and

transfected with plasmid DNA using a modified calcium phosphate method as described previously (Benzing et al., 1999).

Coimmunoprecipitation

Coimmunoprecipitations were performed as described previously (Huber et al., 2001). In brief, HEK 293T cells were transiently transfected and lysed in a 1% Triton X-100 lysis buffer (1% Triton X-100, 20 mM Tris-HCl, pH 7.5, 50 mM NaCl, 50 mM NaF, 15 mM $Na_4P_2O_7$, 2 mM Na_3VO_4, and protease inhibitors) for 15 min on ice. After centrifugation at 15,000 *g* for 15 min and ultracentrifugation at 100,000 *g* for 30 min (both at 4°C), cell lysates containing equal amounts of total protein were precleared with protein G–Sepharose and incubated for 1 h at 4°C with the appropriate antibody followed by incubation with 40 μl protein G–Sepharose beads for ~3 h. The beads were washed extensively with lysis buffer, and bound proteins were resolved by 10% SDS-PAGE. For precipitation of endogenous proteins, mouse kidneys were perfused in situ with ice-cold PBS and homogenized in 1 ml of lysis buffer (20 mM Tris-HCl, pH 7.5, 1% Triton X-100, 25 mM NaF, 12.5 mM $Na_4P_2O_7$, 0.1 mM EDTA, 50 mM NaCl, 2 mM Na_3VO_4, and protease inhibitors). After centrifugation to remove cellular debris, the supernatant was subjected to an ultracentrifugation at 100,000 *g* for 30 min followed by extensive preclearing with protein G–Sepharose. Immunoprecipitation was performed as described previously (Benzing et al., 2001). Coprecipitating proteins were detected after 12% SDS-PAGE of the precipitates and immunoblotting.

Immunofluorescence staining of MDCK, mIMCD3, and human respiratory epithelial cells

MDCK (strain II) or mIMCD3 cells were seeded on coverslips at 100% confluence and cultured for 5–7 d before the experiment. After washing with ice-cold PBS, cells were fixed using 4% PFA, pH 7.5, and 0.05% Triton X-100 for 15 min at room temperature. Cells were washed three times with PBS, and double immunofluorescence staining was performed sequentially with the antibodies as indicated. After washing, slides were incubated with the secondary antibody, Cy2- or AlexaFluor488-labeled anti–rabbit, and Cy3-labeled anti–mouse IgG, washed again, mounted in a commercially available antifade kit (DakoCytomation), and subjected to immunofluorescence microscopy with a microscope (Axiovert200) equipped with the apotome system and a CCD camera (Jena; all were obtained from Carl Zeiss MicroImaging, Inc.) or to confocal microscopy. Confocal images were taken using a laser-scanning microscope (LSM5) equipped with a 100× oil immersion objective (both were obtained from Carl Zeiss MicroImaging, Inc.). The appropriate controls were performed without the first and/or second primary antibodies. In some experiments, the primary antibody was mixed with a 10-fold excess of blocking peptide to proof specific staining. Human respiratory epithelial cells were obtained by transnasal brush biopsy using a cell collector (Cytobrush Plus; Medscand Malmö) and were suspended in RPMI 1640 without supplements. Samples were spread onto glass slides. Cells were fixed with 4% PFA in PBS for 15 min and were permeabilized with 0.2% Triton X-100 in PBS for 5 min before blocking with 0.5% skim milk in PBS overnight. Cells were incubated with primary antibodies and secondary antibodies as described in Results.

To detect GFP-EB1 in cilia, fluorescence images (1,024 × 1,024 pixels) were recorded with a confocal scanning microscope (LSM NLO; Carl Zeiss MicroImaging, Inc.) equipped with a C-Apo 100× NA 1.3 oil immersion objective (Carl Zeiss MicroImaging, Inc.). The scanning speed was set to 0.12 s per image, corresponding to a pixel time of 1.60 μs. The usual pixel size was 0.06 μm in x/y, and the confocal pinhole was set to achieve an optical slice thickness of 0.9 μm. GFP-EB1 was excited at 514 nm, and fluorescence emission was collected above 516 nm.

Immunoelectron microscopy

Freshly isolated mouse trachea was cut into small pieces and immediately transferred to 2.5% PFA in PBS, pH 7.2, for 30 min, washed three times for 10 min in 50 mM ammonium chloride in PBS, and permeabilized with 0.15% Triton X-100 in PBS for 5 min. Incubation with rabbit anti-VHL pAbs for 4 h was followed by washing in PBS four times for 10 min and overnight incubation with the secondary antibodies coupled to 5-nm gold particles (diluted 1:3 in PBS; GE Healthcare). Unbound antibodies were removed by several washings with PBS, and the cells were fixed with glutaraldehyde (2.5%; 50 mM cacodylate buffer, pH 7.2) for 30 min at 4°C. Thereafter, cells were postfixed with 2% OsO_4 for 60 min at 4°C, rinsed with water, dehydrated with ascending alcohol concentrations and propylene oxide, and processed for embedding in Epon. Ultrathin sections were cut with a microtome (Reichert-Jung) and examined with an electron microscope (EM 10A; Carl Zeiss MicroImaging, Inc.).

RNA interference experiments

shRNAs were designed based on the prediction of publicly available prediction programs (Yuan et al., 2004), which are summarized in Table I. shRNAs were cloned into the transient micro-RNA expression vector pcDNA6.2-GW/emGFP/miR (Invitrogen), which coexpresses the shRNA surrounded by miR-155–flanking sequences together with emGFP. To monitor the efficiency of shRNA-mediated knockdown, we created a luciferase reporter construct using psicheck2 (Promega) in which the coding sequence and the 3′ UTR of VHL were fused to the coding sequence of *R. reniformis* luciferase as an artificial 3′ UTR. In addition to *R. reniformis* luciferase, this construct expresses firefly luciferase for internal control. 50 ng of the reporter plasmid was cotransfected with 50 ng of the respective pcDNA6.2-GW/emGFP/miR shRNA construct into HEK 293T cells in a 96-well format using LipofectAMINE 2000 (Invitrogen) as a transfection reagent. *R. reniformis* luciferase and firefly luciferase activities were measured by a dual-luciferase reporter assay system (Promega) in a luminometer (Mithras LB940; Berthold) 24 h after transfection. Transfections and measurements were performed in triplicate. Selected hairpins were GATEWAY cloned into pLenti4/V5/TO/Dest for stable lentiviral expression in mIMCD3 cells.

Confocal laser-scanning microscopy

For fast live cell imaging, cells were seeded on custom-built 35-mm glass-bottom dishes and analyzed the next morning at subconfluent stages. Fluorescence images (512 × 512 pixels) were recorded with a confocal slit scanning microscope (LSM5 LIVE; software 4.0; Carl Zeiss MicroImaging, Inc.) with a C-Apo 63× NA 1.4 oil immersion objective (Carl Zeiss MicroImaging, Inc.) on a heating stage at 37°C in nonperfused condition for 30 s. The scanning speed was set to 0.12 s per image, corresponding to a pixel time of 232 μs; a delay of 500 ms was used between each image. The usual pixel size was 0.2 μm in x/y, and the confocal pinhole was set to achieve an optical slice thickness of 0.9 μm. EB1-GFP was excited at 488 nm, and fluorescence emission was collected above 505 nm. For quantification of the growth direction of microtubules, tracking paths were analyzed for 10 s using MetaMorph software (Universal Imaging Corp.). Tracking paths were measured in one to two square fields (256 μm^2) positioned in the cytosol in a total of 10 independent experiments (VHL negative and positive). As a measure for directed or nondirected movement, the deviation of the individual growth angles from the mean angle was calculated in each square. For better visualization of EB1-GFP dots in the videos, γ adjustment was performed. Statistical analysis was performed for VHL-positive and -negative cells using the two-tailed *t* test.

Online supplemental material

Videos 1 and 2 show representative time-lapse tracings of EB1-GFP fluorescence in VHL-positive (Video 1) and -negative (Video 2) A498 RCC cells. For the mode of data acquisition, refer to the previous section. Fig. S1 shows that pVHL localizes to cilia in respiratory epithelial cells. Fig. S2 shows that cytosolic GFP does not enter the ciliary compartment. Fig. S3 shows that the knockdown of pVHL inhibits the formation of monocilia. Online supplemental material is available at http://www.jcb.org/cgi/content/full/jcb.200605092/DC1.

We thank Christina Engel, Stefanie Keller, Petra Dämisch, and Charlotte Meyer for excellent technical assistance and members of the Benzing and Walz laboratories for helpful discussions. We thank Dr. S.A. Karumanchi (Harvard Medical School, Boston, MA), Dr. D. Trono, Dr. Y. Mimori-Kiyosue, and Dr. L. Naldini for providing cDNAs. We are very grateful to Dr. T. Tuschl and Dr. M. Landthaler for helpful advice in RNA interference experiments and for providing cDNAs and to Dr. J. Eisfeld for help with the imaging experiments.

This study was supported by DFG grants BE 2212, SCHE 1562, SFB 592, and WA 517.

Submitted: 15 May 2006
Accepted: 13 October 2006

References

Benzing, T., and G. Walz. 2006. Cilium-generated signaling: a cellular GPS? *Curr. Opin. Nephrol. Hypertens.* 15:245–249.

Benzing, T., R. Brandes, L. Sellin, B. Schermer, S. Lecker, G. Walz, and E. Kim. 1999. Upregulation of RGS7 may contribute to tumor necrosis factor-induced changes in central nervous function. *Nat. Med.* 5:913–918.

Benzing, T., P. Gerke, K. Hopker, F. Hildebrandt, E. Kim, and G. Walz. 2001. Nephrocystin interacts with Pyk2, p130(Cas), and tensin and triggers phosphorylation of Pyk2. *Proc. Natl. Acad. Sci. USA*. 98:9784–9789.

Esteban, M.A., S.K. Harten, M.G. Tran, and P.H. Maxwell. 2006. Formation of primary cilia in the renal epithelium is regulated by the von Hippel-Lindau tumor suppressor protein. *J. Am. Soc. Nephrol.* 17:1801–1806.

Etienne-Manneville, S., and A. Hall. 2003. Cdc42 regulates GSK-3beta and adenomatous polyposis coli to control cell polarity. *Nature*. 421:753–756.

Fan, S., T.W. Hurd, C.J. Liu, S.W. Straight, T. Weimbs, E.A. Hurd, S.E. Domino, and B. Margolis. 2004. Polarity proteins control ciliogenesis via kinesin motor interactions. *Curr. Biol.* 14:1451–1461.

Fukata, M., T. Watanabe, J. Noritake, M. Nakagawa, M. Yamaga, S. Kuroda, Y. Matsuura, A. Iwamatsu, F. Perez, and K. Kaibuchi. 2002. Rac1 and Cdc42 capture microtubules through IQGAP1 and CLIP-170. *Cell*. 109:873–885.

Gnarra , J.R., K. Tory, Y. Weng, L. Schmidt, M.H. Wei, H. Li, F. Latif, S. Liu, F. Chen, F.M. Duh, et al. 1994. Mutations of the VHL tumour suppressor gene in renal carcinoma. *Nat. Genet.* 7:85–90.

Gundersen, G.G., E.R. Gomes, and Y. Wen. 2004. Cortical control of microtubule stability and polarization. *Curr. Opin. Cell Biol.* 16:106–112.

Hergovich, A., J. Lisztwan, R. Barry, P. Ballschmieter, and W. Krek. 2003. Regulation of microtubule stability by the von Hippel-Lindau tumour suppressor protein pVHL. *Nat. Cell Biol.* 5:64–70.

Huber, T.B., M. Kottgen, B. Schilling, G. Walz, and T. Benzing. 2001. Interaction with podocin facilitates nephrin signaling. *J. Biol. Chem.* 276:41543–41546.

Igarashi, P., and S. Somlo. 2002. Genetics and pathogenesis of polycystic kidney disease. *J. Am. Soc. Nephrol.* 13:2384–2398.

Iliopoulos, O., A. Kibel, S. Gray, and W.G. Kaelin Jr. 1995. Tumour suppression by the human von Hippel-Lindau gene product. *Nat. Med.* 1:822–826.

Jaffe, A.B., and A. Hall. 2005. Rho GTPases: biochemistry and biology. *Annu. Rev. Cell Dev. Biol.* 21:247–269.

Kaelin, W.G., Jr. 2003. The von Hippel-Lindau gene, kidney cancer, and oxygen sensing. *J. Am. Soc. Nephrol.* 14:2703–2711.

Kaelin, W.G., Jr. 2004. The von Hippel-Lindau tumor suppressor gene and kidney cancer. *Clin. Cancer Res.* 10:6290S–6295S.

Lolkema, M.P., N. Mehra, A.S. Jorna, M. van Beest, R.H. Giles, and E.E. Voest. 2004. The von Hippel-Lindau tumor suppressor protein influences microtubule dynamics at the cell periphery. *Exp. Cell Res.* 301:139–146.

Lubensky, I.A., J.R. Gnarra, P. Bertheau, M.M. Walther, W.M. Linehan, and Z. Zhuang. 1996. Allelic deletions of the VHL gene detected in multiple microscopic clear cell renal lesions in von Hippel-Lindau disease patients. *Am. J. Pathol.* 149:2089–2094.

Lutz, M.S., and R.D. Burk. 2006. Primary cilium formation requires von hippel-lindau gene function in renal-derived cells. *Cancer Res.* 66:6903–6907.

Mandriota, S.J., K.J. Turner, D.R. Davies, P.G. Murray, N.V. Morgan, H.M. Sowter, C.C. Wykoff, E.R. Maher, A.L. Harris, P.J. Ratcliffe, and P.H. Maxwell. 2002. HIF activation identifies early lesions in VHL kidneys: evidence for site-specific tumor suppressor function in the nephron. *Cancer Cell*. 1:459–468.

Mimori-Kiyosue, Y., N. Shiina, and S. Tsukita. 2000. The dynamic behavior of the APC-binding protein EB1 on the distal ends of microtubules. *Curr. Biol.* 10:865–868.

Nauli, S.M., F.J. Alenghat, Y. Luo, E. Williams, P. Vassilev, X. Li, A.E. Elia, W. Lu, E.M. Brown, S.J. Quinn, et al. 2003. Polycystins 1 and 2 mediate mechanosensation in the primary cilium of kidney cells. *Nat. Genet.* 33:129–137.

Palazzo, A.F., T.A. Cook, A.S. Alberts, and G.G. Gundersen. 2001. mDia mediates Rho-regulated formation and orientation of stable microtubules. *Nat. Cell Biol.* 3:723–729.

Pan, J., Q. Wang, and W.J. Snell. 2005. Cilium-generated signaling and cilia-related disorders. *Lab. Invest.* 85:452–463.

Praetorius, H.A., and K.R. Spring. 2003a. Removal of the MDCK cell primary cilium abolishes flow sensing. *J. Membr. Biol.* 191:69–76.

Praetorius, H.A., and K.R. Spring. 2003b. The renal cell primary cilium functions as a flow sensor. *Curr. Opin. Nephrol. Hypertens.* 12:517–520.

Ratcliffe, P.J. 2003. New insights into an enigmatic tumour suppressor. *Nat. Cell Biol.* 5:7–8.

Rosenbaum, J.L., and G.B. Witman. 2002. Intraflagellar transport. *Nat. Rev. Mol. Cell Biol.* 3:813–825.

Salaycik, K.J., C.J. Fagerstrom, K. Murthy, U.S. Tulu, and P. Wadsworth. 2005. Quantification of microtubule nucleation, growth and dynamics in wound-edge cells. *J. Cell Sci.* 118:4113–4122.

Schoenfeld, A., E.J. Davidowitz, and R.D. Burk. 1998. A second major native von Hippel-Lindau gene product, initiated from an internal translation start site, functions as a tumor suppressor. *Proc. Natl. Acad. Sci. USA*. 95:8817–8822.

Snell, W.J., J. Pan, and Q. Wang. 2004. Cilia and flagella revealed: from flagellar assembly in Chlamydomonas to human obesity disorders. *Cell*. 117:693–697.

Srayko, M., A. Kaya, J. Stamford, and A.A. Hyman. 2005. Identification and characterization of factors required for microtubule growth and nucleation in the early *C. elegans* embryo. *Dev. Cell*. 9:223–236.

Watanabe, T., S. Wang, J. Noritake, K. Sato, M. Fukata, M. Takefuji, M. Nakagawa, N. Izumi, T. Akiyama, and K. Kaibuchi. 2004. Interaction with IQGAP1 links APC to Rac1, Cdc42, and actin filaments during cell polarization and migration. *Dev. Cell*. 7:871–883.

Yuan, B., R. Latek, M. Hossbach, T. Tuschl, and F. Lewitter. 2004. siRNA Selection Server: an automated siRNA oligonucleotide prediction server. *Nucleic Acids Res.* 32:W130–W134.